PUB-16-042-PPD
ACCEPTED

# High time-resolution photodetectors for PET applications

Anatoly Ronzhin,

*Fermilab, Batavia, Il 60510, USA*

**Abstract**

This article describes recent developments aiming at the improvement of the time resolution of photodetectors used in positron emission tomography (PET). Promising photo detector candidates for future PET-time-of-flight (TOF) applications are also discussed.

*Keywords:*

Positron emission tomography; Time of flight; Silicon photomultipliers.

## 1. Introduction

The use of time of flight (TOF)in positron emission tomography (PET) was initially proposed in the 1960s[1], although the first TOF-PET system prototype was developed only later, in 1982[2].A detailed review of PET research (including TOF-PET) is provided in Reference [3].Photomultipliers (PMTs) with moderate timing properties are currently used in "old-style" PET scanners[4]; on adding a TOF measurement to the currently available commercial PET scanners, the image signal-to-noise ratio (SNR) and contrast can be improved markedly with a coincidence time resolution (CTR) only around 600 ps [5]. Prototypes of scanners with microchannel plates (MCP-PMT) as photodetectors and a superior time resolution (TR) are still at the research and development stage [6, 7].As MCP-PMTs are sensitive to magnetic fields, silicon photomultipliers (SiPMs) have become the focus of study for TOF-PET application [8-11].

Operated by Fermi Research Alliance, LLC under Contract No. De-AC02-07CH11359 with the United States Department of Energy.

The sensitive area of current SiPM (from 1x1 $mm^2$ upto5×5 $mm^2$) matches well the size of the crystals used in PET, which is not the case for conventional PMTs. Being solid-state devices, SiPMs are not sensitive to magnetic fields and possess excellent timing characteristics; this facilitates the combination of TOF-PET scanners with magnetic resonance imaging (MRI) scanners. This proposed combined device (TOF-PET–MRI) is a powerful diagnostic tool for discovering early-stage cancers.

The paper is organized as follows. The various sources of time jitter of photodetectors used in the TOF-PET scanners and prototypes are described in section 2. Special attention is taken to the scintillators used in PET as one of the main source of the time jitter. The photodetectors PMTs, MCP-PMTs, and SiPMs used in TOF-PET scanners and prototypes are described in sections 3, 4, and 5, respectively. The conclusions are presented in section 6.

**2. Time jitter of the photodetectors used in TOF-PET.**

In PET, the photodetector output response is a convolution of the scintillation light pulse (photons time distribution in time) with the signal shape of the photodetector. The convolution results in an output signal with fast rise time if scintillator has fast rise time (even with a long tail). The photodetector must be very fast (very sharp rise time and fall time, e.g. MCP) in this case.

The situation is totally different if photodetector has fast rise time and long tail. In this case the convolution will result in response with much larger rise time (even if both scintillator and photodetector have very fast rise time). We verified this behavior many times experimentally and in agreement with our calculations. This is the reason why when we use SiPM (fast rise time and long tail) for PET we trimming the SiPM signal by a clipping capacitance to get fast rise time of the output signal. This is the case of PET when the scintillator is the source of the

light. The fast rise time of the output signal plays a dominant role in all our time measurements.

The gamma ray photons to be detected enter the crystal at the speed of light and, when interacting with the crystal, produce a flash of scintillation light. The time between the entry of the photon into the crystal and the first interaction is the initial source of the time jitter; the time associated with the conversion of the incident photon into scintillation adds to the spread. The scintillation light travels from the point of interaction to the photo detector with a velocity $c/n$, where $n$ is the effective refractive index of the crystal and $c$ is the speed of light in vacuum. The time taken by the scintillation light to travel to the photo detector is the next source of a time spread. With a typical speed of light propagation inside the crystal of ~7 ps/mm, even a 10 mm long crystal produces an additional time spread around 70 ps.

This is an example that illustrates the influence of crystal length on the time spread. The time jitter due to the crystal length could be suppressed by using a special readout (e.g. two photodetectors looking at the same crystal from opposite side).

It is evident that the bouncing of the light from side of the crystal could also increase the time jitters of the additionally collected photons. Hence the light increase by wrapping the crystal sides does not necessarily lead to an improvement of the timing of the whole system. In general the time jitter is smaller for the light directly reaching the photodetector.

When the scintillation light reaches the photo detector, the photons are converted into an electrical signal, producing an additional time jitter. The magnitude of the jitter depends on the timing parameters of the incident light on the photo detector, the time response (signal) of the photo detector to the light, and a

time jitter associated with a part of the signal chosen for “triggering”, called the “time stamp.” This last factor depends on the algorithm used to detect the signal.

In general the shape of the signal provided by a photo detector has two main components: the signal rise time, $T_r$, and fall time, $T_f$. The time stamp is usually selected to be at the leading edge of the signal.

The noise is another important parameter of the photodetectors used in the time measurements. The signal to noise ratio (SNR) is also an important factor to determine the time response of the detector; signal and noise can be measured in direct current and alternating current modes, or, alternatively, in units of current, number of electrons, mV, etc.

The single photoelectron time resolution (SPTR) is another main timing parameter of all photodetectors. It represents the time jitter initiated by single photon hitting the photodetector. The SPTR allows to make an estimation of time spread for the whole system that measure the timing.

In any TOF systems, two photons are detected from the opposite sides of the ring; the time jitter between these signals is referred to as coincidence time resolution (CRT).The CTR depends on all of the above mentioned parameters, including the time stamp, defined as the point on the signal with the smallest timing fluctuation. The time stamp also depends on the front-end of the used electronics. Waveform digitizers are currently used to perform timing analyses of the signals [14]; unlike front end electronics that operate at the data collection level, these digitizers allow off-line signal analysis. Different algorithms can be applied to the signal timing analysis with the digitizers, producing different TRs.

D. Schaart and his group and P. Lecoq and his group made simulations and experimental study of the CTR on PET. One of their main conclusions is that further improvement of the CTR could be obtained by a light yield increase and a timing

improvement of the scintillator t. The search continues for very fast, high light yield and not very expensive scintillators.

**3. Spatial and time resolution of PET scanners with PMT.**

PET scanners record the time coincidence between two photons produced back to back after positron emission from a radionuclide-tagged tracer molecule[15];the TOF-PET scanner measures also accurately the time difference between the two photons. One of the measured values is the CTR. A PET scanner consists of several crystals coupled with photodetectors; each crystal–photo detector pair constitutes the basic element of the scanner, arranged in the form of a ring. The CTR is significantly dependent on the properties of the crystal (light yield and timing).

The physical size of the scanner element as a noticeable effect on its spatial resolution. Smaller elements clearly produce better spatial resolution However, a size below ~2 mm is not practical [16]. The earliest PMTs used in PET had a sensitive area of typically 5cmin diameter, considerably larger than the crystal size used; even PMTs with smaller sensitive area are too large to match the crystal size adequately. Different methods have been used to improve the spatial resolution in PET, for example, a geometry where several PMTs share the light from the crystals [17].

The most straightforward method of improving the spatial resolution is to use small-size PMTs that adequately match the size of the crystals. Despite these advantages, this method is not practical as the scanner is expensive. As the smallest PMT diameter used currently is~10 mm, multichannel position-sensitive PMTs can be used to better match a smaller crystal size [18].

As noted earlier, the main parameters of photodetectors for TOF-PET application are signal shape, noise, and SPTR. Examples of the PMT signal shape are shown in Fig. 1. The rise and fall times of the signals, determining the output

pulse duration, are of the order of a few nanoseconds. In fact, a shorter PMT signal results in a superior TR and better performance at high counting rates.

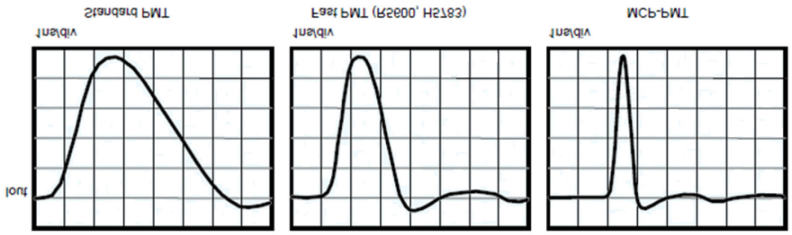

Fig. 1. Examples of signal shape of different PMTs.

| PMT | PMT Gain | FWHM | Iser | Vout (50 Ω) | Imax (cont) | I max (pulse) |
|---|---|---|---|---|---|---|
| Standard | $10^7$ | 5 ns | 0.32 mA | 16 mV | 100uA | 50mA |
| Fast PMT | $10^7$ | 1.5 ns | 1 mA | 50 mV | 100uA | 100mA |
| MCP PMT | $10^6$ | 0.36 ns | 0.5mA | 25 mV | 0.1uA | 10mA |

Table 1: Typical PMT parameters

As it can be seen in Table 1, the PMT signal for one photon is of few tens of millivolts on 50 Ω, easily larger than the noise produced by most electronic recording devices, thus permitting detection of single photons.

The peak current even for a single electron response, $I_{ser}$, is larger than the maximum continuous output current, $I_{max}$; therefore, a continuous light signal does not produce a continuous current at the output, but a train of random single electron response pulses. The PMT noise predominantly consists of single photoelectrons. The PMT signal in PET is much higher than the noise produced, which suggests that the PMT noise does not have a significant effect on the TR. The TR for PET with a fast PMT could be of the order of 350 ps [19].

**4. MCP-PMTs**

The micro-channel plate photomultiplier (MCP-PMT) is a ~ 1 mm thick slab of a highly resistive material fabricated packing a dense set of tiny tubes over the entire surface from one face to the opposite side. The photocathode is deposited on the upper face, and the amplified charge collected on pads and strips at the bottom

side. The microchannel (or pore) diameter ranges from 10 to 50 μm for large area picosecond photo detector (LAPPD) MCPs [20].Ultrafast MCP-PMTs are described in Ref. [21].

PET scanners with MCP-PMTs have superior TR due to the excellent timing properties of MCP-PMTs. Examples of the signal shapes recorded with commercial fast MCP-PMT are shown in figs. 2 and 3.Fig. 4shows the measured SPTR for the Hamamatsu R3809U-50 MCP-PM. The main peak has 25 ps FWHM; the bump observed in the time distribution is caused by the electron backscatter from the front MCP. The SPTR measured for the Photek 240 is approximately 30 ps. [22].

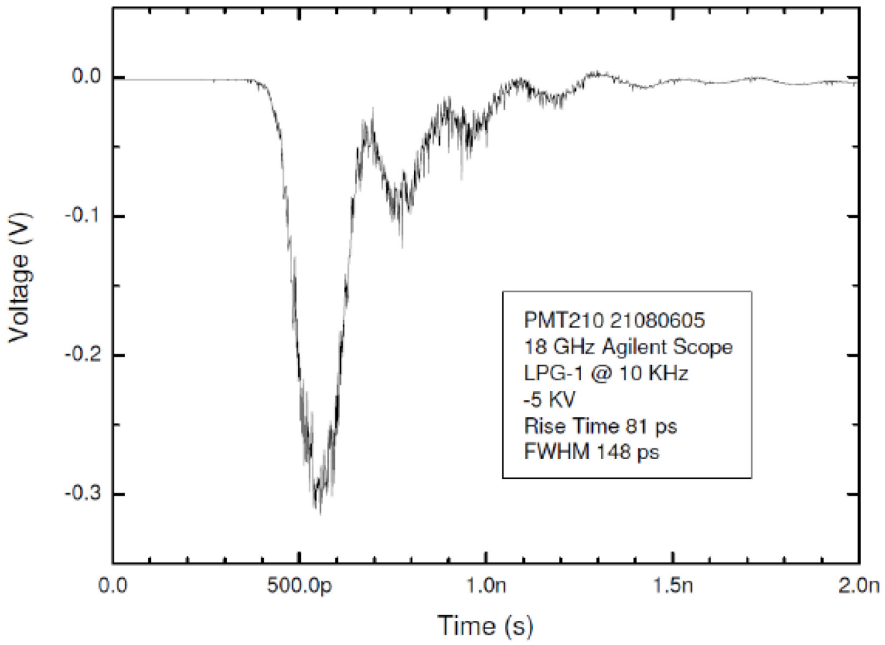


Fig. 2. Signal shape of the Photek 210.

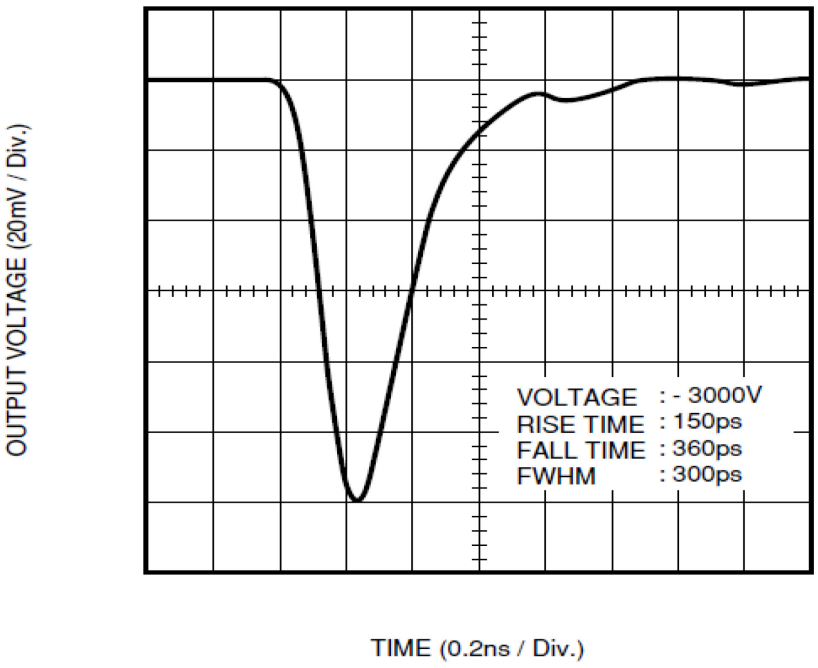


Fig. 3. Signal shape of the Hamamatsu R3809U-50 MCP-PMT.

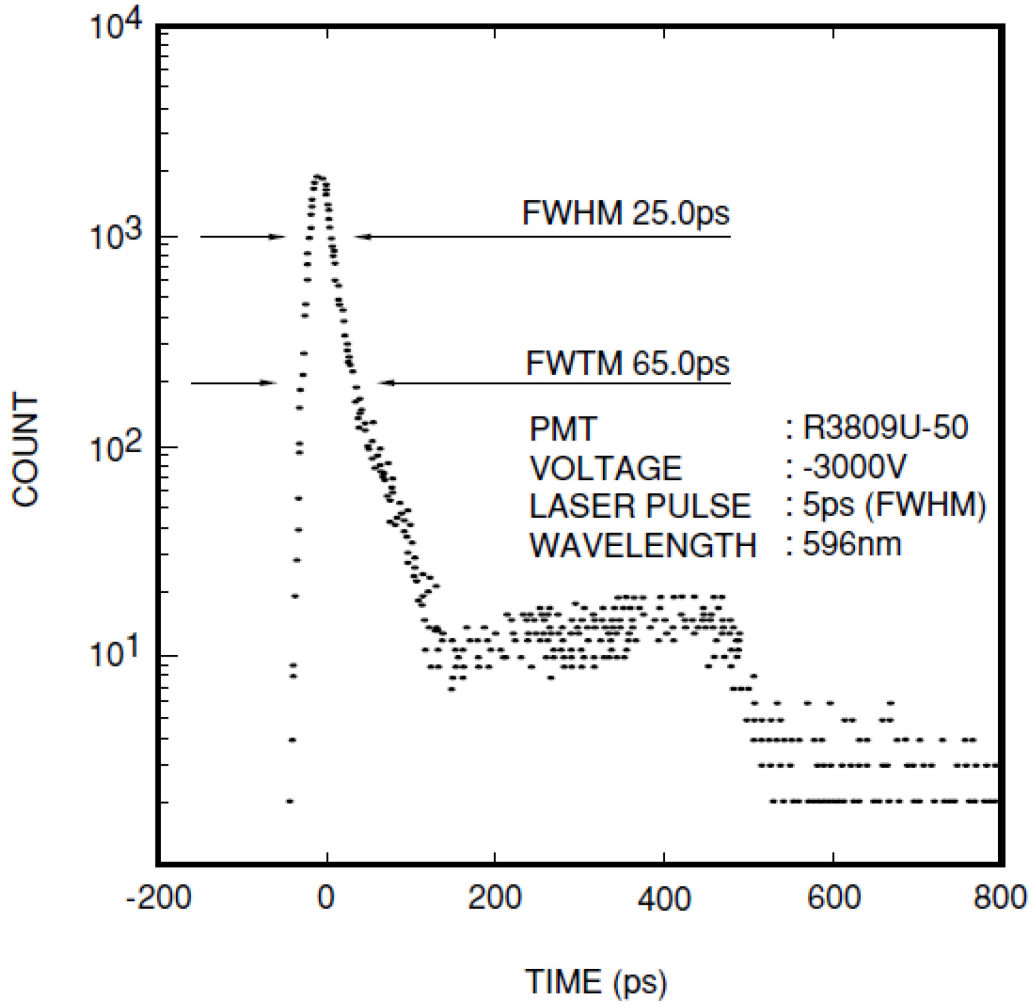


Fig. 4. The SPTR-for the Hamamatsu R3809U-50 MCP-PMT.

Very promising results were obtained for the MCP-PMT developed by the LAPPD collaboration, with a sensitive area of 8”x8” [20]. The goal of the project is to achieve a TR of 1 ps for ~100 photoelectrons produced by Cherenkov radiation; the development also aims at obtaining a CTR of 100 ps for PET scanners. It was shown by the LAPPD team (experimentally and by modeling) that the smaller is the pore size, the closer is the location of the MCPs to the photocathode (PC) and the higher electric field between the PC and the MCP that leads to a better TR [20]. The LAPPD MCP, the top view, the elements of the pore configuration, and the bottom

view are presented in fig. 5; an assembled MCP PMT with a strip-line readout is shown in Figure 6.

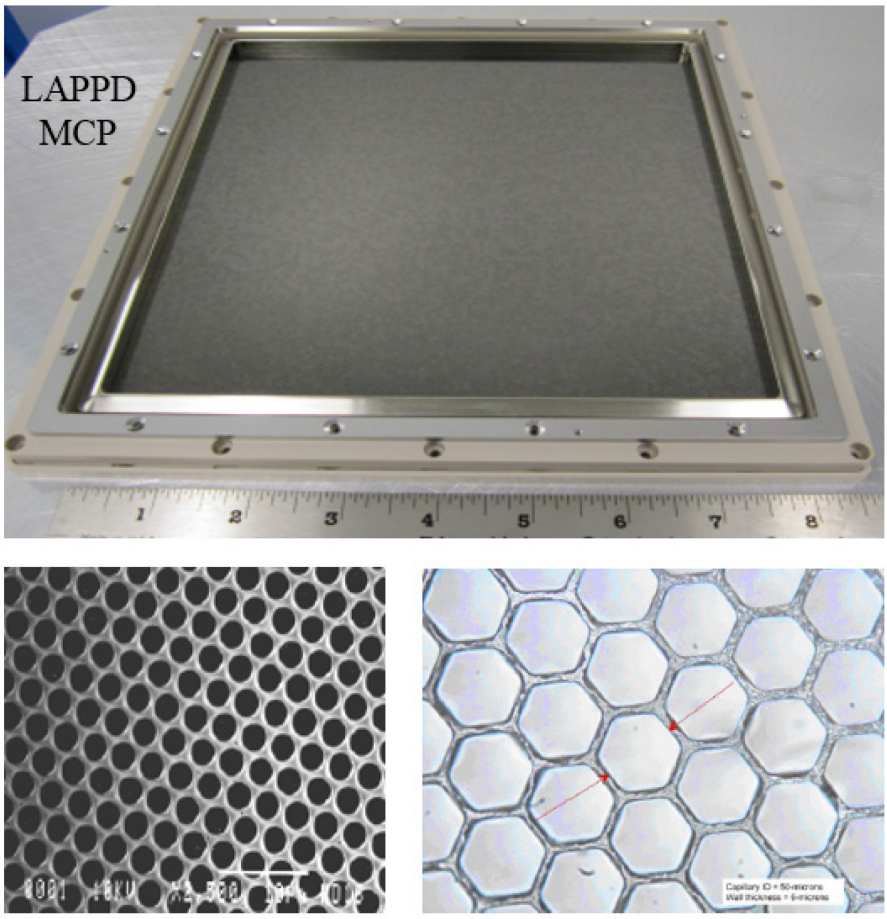


Fig. 5. LAPPD MCP, top view, elements of the pore configuration, bottom view.

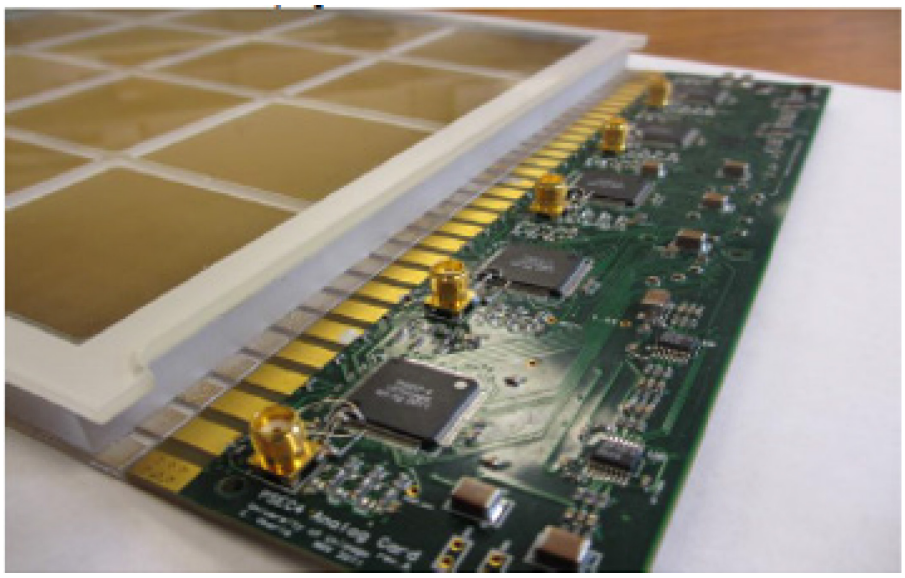

Fig. 6. View of a LAPPD MCP-PMT with strip-line readout.

The LAPPD MCP is made of borofloat glass. The sensitive area is 8”x8”, the thickness is 1.2mm, the pore size is 20 mm. An applied HV of 1 kV allows to obtain a gain up to $10^4$. Atomic layer deposition (ALD) method used to activate the pores inner surface of the MCP. Resistive coating of the pore is ~100nm of the thickness of the layer and emissive coating is ~ 20nm. The noise of the MCP is <0.1 counts $cm^{-2}$ $s^{-1}$.

Fig. 7 shows the dependence of TR on SNR, measured using a picosecond laser and a strip line as readout [20].

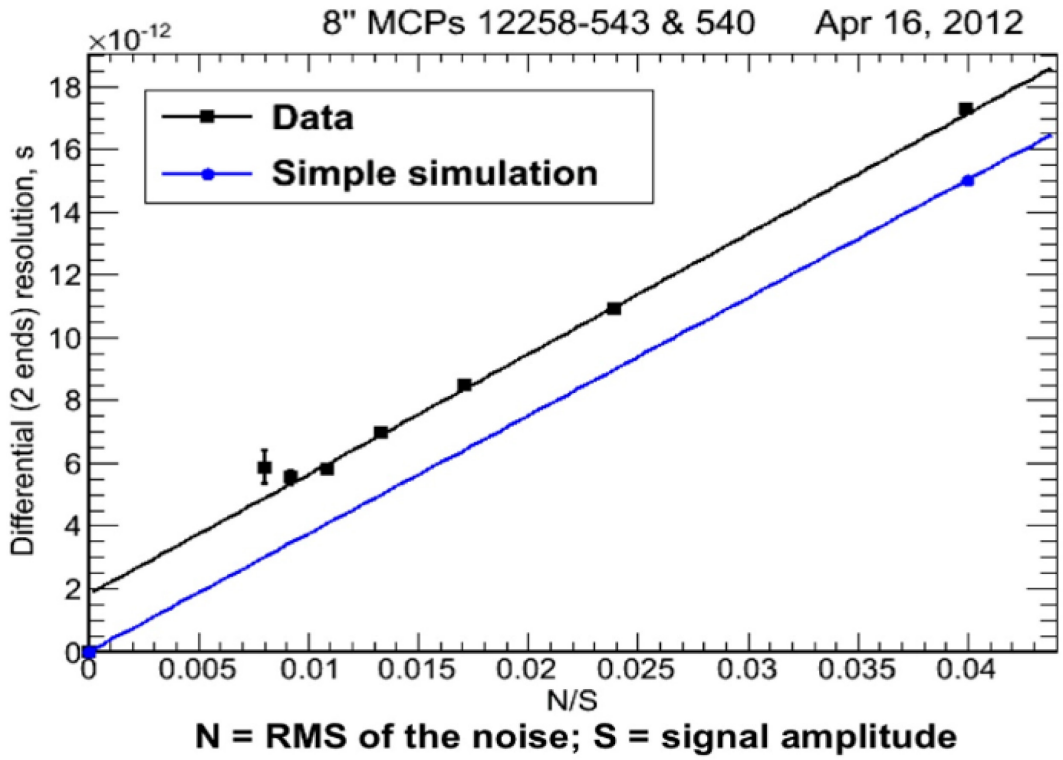


Fig 7. Dependence of the TR on signal over noise ratio for an 8"x8" MCP [20]. The strip line bandwidth used in the measurements is 1.6 GHz.

Below are a few main results already obtained by the LAPPD project. The MCP-PMT quantum efficiency for blue light is > 20% (200 x 200 $mm^2$ of the sensitive area). The time resolution for the single photoelectron is ~ 50 ps. Many tests have been carried out to study the MCP performance: gain, uniformity, stability, ageing. All of them show very promising results for future application.

**5. SiPMs**

The SiPM shows a great promise as a photo detector for application in TOF-PET [22, 23] due to its excellent timing properties. The avalanche development in a single cell of SiPM involves photon absorption, impact ionization, electron–hole pair creation, and longitudinal buildup of the avalanche due to the acceleration of electrons (or holes) in the high electric field (~ 3–5 × $10^4$V/mm). The avalanche builds up along about 1 μm on the photoelectron path, in line with the next

transversal avalanche development. The time jitter starting from photon absorption to the carrier creation can be excluded from the model. The time taken for the avalanche to build up along the electric field is about 10 ps, and transversal time spread is ~100 ps [24]. The measured transverse size of the avalanche is ~10 μm in diameter, independent of the overvoltage that is defined as the difference between the bias voltage applied to SiPM and the breakdown voltage.

The SPTR of the SiPMs is almost the same for blue and red light (3 and 2 eV), both for the n-on-p or p-on-n structures; the SPTR ranges from 50 to 70 ps depending on the SiPM pixel size. The presence of a high electric field (ranging from 1 to 10 μm) closer to the silicon surface does not significantly affect the SPTR [24].Therefore, most of the SiPM time spread is caused by a single photoelectron (SPTR) that triggers the transverse development of the avalanche in the high electric field. The speed of the transverse development is estimated to be ~10 ps/μm [24]. This corresponds to the location of the high electric field on the silicon surface (< 1 μm) and depends on the value of the polysilicon quenching resistor used. SiPMs can easily detect a single photoelectron [25].

The SPTR can be measured using a PiLas laser as generator [26]; the distribution of the time difference between the two signals permits to deduce the intrinsic TR of the sensor from the expression:

$$\sigma_{total} = \text{sqrt}\,(\sigma^2_{detector} + \sigma^2_{electrical}) \qquad (1)$$

where $\sigma_{det}$ and $\sigma_{electr}$ are the time jitters introduced by the detector and electronics, respectively.

The “electrical” TR can be measured as the time jitter between the start and the stop signal generated by the same signal source. Waveform digitizers are currently used for conducting timing analyses, allowing off-line signal analysis.

Different algorithms are applied to signal timing analysis with the DRS4 resulting in different TR [27]. The contribution of the electrical TR to the total TR

of most of the TOF-PET devices currently used, including waveform digitizers, can be neglected, as they are only a few picoseconds. A new DRS4 calibration method produces an electrical TR of ~2 ps, even with a 200-ps sampling [28].

A TOF-PET scanner prototype using SiPMs as photo detectors producing a CTR of ~100 ps have been developed [8]. This prototype was found to best match the small crystal size ($3 \times 3 \times 5$ mm$^3$).

SiPMs with LYSO crystals ($3 \times 3 \times 15$ mm$^3$) for application in TOF-PET were studied. A CTR ranging from 175 to 188 ps, FWHM, was obtained with the DRS4 waveform digitizer in this study (Fig. 8)[29].

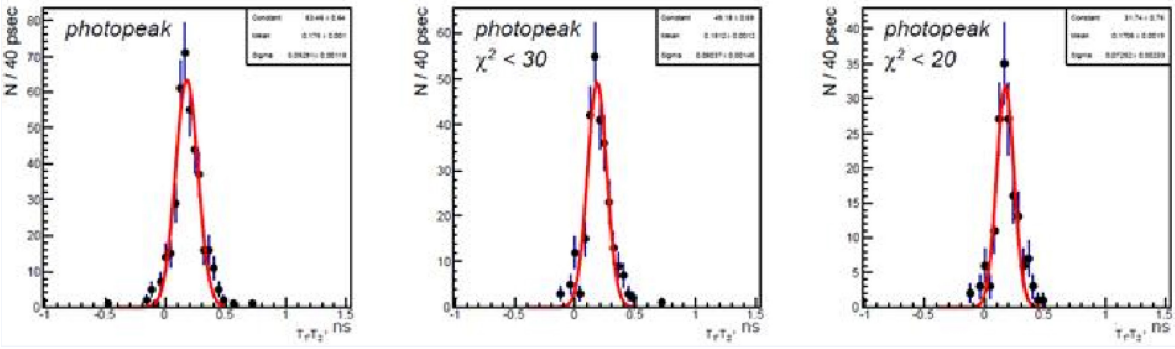


Fig. 8. Examples of CTR distributions. The values 240, 188, and 175 ps (FWHM), correspond to different chosen efficiencies (see the main text)[29].

A full-scale clinical TOF-PET scanner can be developed cost-effectively by combining the described approach [29] with a strip-line readout [30]. The proposed scanner can obtain a spatial resolution of~1 mm, which is close to the intrinsic limit of the technique [31]. The TR of TOF-PET can be further enhanced if some of the photo detector timing parameters are attained; e.g. SPTR ~10 ps, counting rate >100 MHz. Fast-timing scintillators are another research avenue for improving TOF-PET TRs.

**6. Conclusion.**

The use of TOF in PET is a well-established method of improving image quality in clinical scanners. The TOF-PET technique currently used in research and development presents a CTR of ~100 ps, which can become a standard for industrial scanners in the future.

With their intrinsic low noise and single photon sensitivity, MCP or SiPM-based TOF-PET scanners are a very promising tool in medical diagnostics, potentially capable of better image quality and shorter scanning times.

**Acknowledgements.**

I would like to express my deep appreciation to Professor Fabio Sauli for his big efforts to improve the initial version of the article. I appreciate Professor Alberto Del Guerra and reviewer work to improve the article.

## References

1. H. O.Anger, J. Nuclear Medicine ISA Trans. 1966, 5 (4), p. 311.
2. Michel Ter-Pogossian et al., Journal of Computer Assisted Tomography, 6, 1982, pp.125-133.
3. Gerd Muehllehner and Joel S Karp, Phys. Med. Biol. 51 (2006), R117–R137.
4. J. Karp et al., Journal Nuclear Medicine. 49(3), (2008), p. 462.

5. T. K. Lewellen, Seminar Nuclear Medicine. vol. 28, 1990, pp. 268–275.

6.Kim H et al.,NIM, A. 622(3),(2010) pp. 628-636.

7. Kim H et al., NIM, A. 662(1), (2012) pp. 26-32.

8. D. R. Schaart et al., Physics Med. Biol., 55 (2010) pp. 179–189.

9. P. Jarron et al., IEEE Transaction on Nuclear Science, Vol. 58, No. 3, 2011, p. 597.
10. C. Piemonte et al, IEEE Transactions on Electron Devices, , 2013, p. 2567.
11. A. Ronzhin et al., NIM, A703 (2013), pp. 109–113
12. H. Kim et al., NIM, A784 (2015), pp. 557.
13. A. Ronzhin. 2013 IEEE Nuclear Science Symposium Conference Record NPO1-1, 2013.
14. S. Ritt.NIM, A518, 2004, pp. 470-471.
15. S. Surti et al.,*J. Nucl.Med.*,vol. 48, 2007, pp. 471–480.
16. W. Moses, Wand Ullisch. IEEE Trans. Nucl. Sci. 53,year, pp. 78–85.
17. S. Liu at al., IEEE Trans Nucl. Sci. 56, 2009, pp. 2614-2620.
18. Yiping Shao et al. Nuclear Science Symposium and Medical Imaging Conference Record, V.2., 1995, pp. 1055 – 1059.
19. Christopher et al., IEEE Nuclear Science Symposium Conference, Record M22-4, 2007.

20. B. Adams et al.,NIM, A732 (2013) p. 392.
21. C. J. Horsfield et al., Rev. Sci. Instrum. 2010 Oct. 81 (10): 10D 318.
22. 15. A. Ronzhin et al., NIM, A 623 (2010) pp. 931–941.
23.C. Piemonte et al., IEEE Trans. on Electron Devices, Vol, ,2013pp. 2567 – 2573.
24. E. Popova et al.,http://www.astro.uniwuerzburg.de/~tbretz/Talk_N8-3.PDF
25. A. Ronzhin et al., NIM, A 616 (2010), pp. 38-44.
26. Pilas picosecond laser system, http://www.alsgmbh.com/pilas.htm
27. A. Ronzhin et al., NIM, A 668, (2012) pp. 94-97.
28. H. Kim et al., NIM, A 767 (2014), pp. 67-74.
29. A. Ronzhin et al., NIM, A703 (2013), pp. 109-113.

30. H. Kim et al., IEEE Nuclear Science Symposium Conference Record 2012, 1025,

31. S. Seifert et al. Physics Med. Biol., 58(9), 2013, pp. 3061-3074.